2017

Computational Fluid Dynamics Study of Thromboembolism as a Function of Shunt Size and Placement in the Hybrid Norwood Palliative Treatment of Hypoplastic Left Heart Syndrome

John Seligson
University of Central Florida

COMPUTATIONAL FLUID DYNAMICS STUDY OF THROMBOEMBOLISM AS A FUNCTION OF SHUNT SIZE AND PLACEMENT IN THE HYBRID NORWOOD PALLIATIVE TREATMENT OF HYPOPLASTIC LEFT HEART SYNDROME

by

JOHN M. SELIGSON
B.S. University of Central Florida, 2015

A thesis submitted in partial fulfillment of the requirements
for the degree of Master of Science
in the Department of Mechanical and Aerospace Engineering
in the College of Engineering and Computer Science
at the University of Central Florida
Orlando, Florida

Spring Term

2017

Major Professor: Alain Kassab

ABSTRACT

The Hybrid Norwood procedure has emerged as a promising alternative palliative first stage treatment for infants with Hypoplastic Left Heart Syndrome (HLHS). The procedure is done to provide necessary blood flow to the pulmonary and systemic regions of the body. The procedure can affect hemodynamic conditions to be pro-thrombotic, and thrombus particles can form and release from the vessel walls and enter the flow. Assuming these particles are formed and released from the shunt surface, a Computational Fluid Dynamics (CFD) model can be used to mimic the patient's vasculature geometry and predict the occurrence of embolization to the carotid or coronary arteries, as well as the other major arteries surrounding the heart. This study used a time dependent, multi-scale CFD analysis on patient-specific geometry to determine the statistical probability of thrombus particles exiting each major artery. The geometries explored were of a nominal and patient specific nature. Cases of 90% and 0% stenosis at the aortic arch were analyzed, including shunt diameters of 3mm, 3.5mm, and 4mm. Three different placements of the shunt were explored as well. The intent of this study was to suggest best methods of surgical planning in the Hybrid Norwood procedure by providing supporting data for optimal stroke and myocardial infarction prevention.

To my wife, Jana,

for the gift you are to me,

and the wonderful love you show.

I love you very much.

ACKNOWLEDGMENTS

I would like thank Dr. Alain Kassab for bringing me through this journey in research. In education, I have learned much. In skill, I have gained more. I would not be on the path I am on today if it were not for his direction and teaching. I am a better engineer and researcher, and for that I am thankful.

To Ray Prather, for his invaluable assistance in working with the LPM. I could not have gained proficiency in so short a time without your great working knowledge of the model. Thank you for taking time out of your day to teach and equip me for success.

To Dr. Eduardo Divo, Dr. William DeCamplli, and Dr. Hansen Mansy, thank you for giving your time, effort, and advice through this process. I have benefited greatly from your knowledgeable input and critique.

To my grandmother, Diana Boyce, who loved me and supported me during my last semesters of school. Thank you for helping me make wise decisions, for reassuring me during difficult times, and for being the best grandmother and a wonderful friend. I love you.

TABLE OF CONTENTS

LIST OF FIGURES

LIST OF TABLES

CHAPTER ONE: INTRODUCTION

Hypoplastic Left Heart Syndrome (HLHS) is a congenital heart disease marked by several myocardial growth defects, including severe underdevelopment of the left ventricle. These malformations greatly affect normal blood flow through the heart as well as to the rest of the body. The Hybrid Norwood procedure has proven to be a viable option to treat newborns by a sequence of surgeries aimed at redirecting most of the workload onto the right ventricle while simultaneously relieving the right ventricle of pulmonary circulation. The addition of a shunt sutured at the top of the artificial aortic arch that releases flow at the root of the innominate artery reinstates blood flow to the cerebral and brachial arteries in case of severe distal aortic arch stenosis.

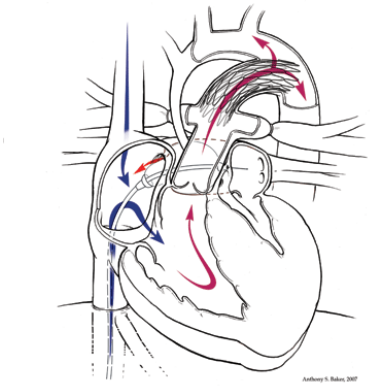

Figure 1: Hybrid Norwood Stage 1 Geometry (Nationwide Children's)

Over the past seventeen years, the hybrid procedure has often been a preferred method to stage I palliation. Its results in survival can be equivalent to that of stage I palliation, and similar to conventional palliation. The subsequent growth of the pulmonary arch along with its

hemodynamic environment are comparable to pre-stage II. Ventricular function is also well preserved with hybrid palliation. The method requires less resources and postoperative recovery is relatively shortened. The goal of the Hybrid Norwood procedure is to create unhindered pulmonary flow, systemic flow, and intra-atrial communication. By placing bilateral pulmonary artery bands and a ductal stent, this outcome is possible (Honjo and Caldarone 103).

The conventional method was first proposed and implemented by Dr. William Norwood, but the hybrid method was unavailable until stenting was clinically possible. In the early 1990s, animal studies suggested success of using stents, and by 2002, Akintuerk et al. performed the first reported success of the hybrid method in which 87.5% of patients resulted positively (Honjo and Caldarone 104) (Akintuerk et al. 1101). This method is not a permanent solution, but rather a temporary palliation until the final two stages are performed. The procedure is not completely effective for all patients, with average results of 80% positive (Ruiz et al. 1605).

The procedure for the Hybrid Norwood surgery involves several steps. Polytetrafluoroethylene banding is applied to each branch of the pulmonary artery in order to balance systemic and pulmonary flow. Usually, echocardiography is used to measure the tightness of the bands, to ensure a specific value. These bands are to reduce flow through the pulmonary arteries and balance flow to the rest of the body. A stent is then placed in the ductus arteriosus to allow systemic flow. Balloon atrial septostomy is then performed to open the septum between the atria, allowing non-oxygenated blood to mix with oxygenated blood (Brescia et al. 1778). In cases where there is no atrial septal defect, this concludes stage I. After recovery, the patient would then undergo stage II at 4 to 6 months and stage III, or Fontan procedure, at age 2. Stage II includes

removal of the ductus arteriosus stent and pulmonary artery bands, joining of the aorta with the pulmonary root, and connection of the superior vena cava to the pulmonary artery. Stage III includes rerouting the inferior vena cava to the pulmonary artery (Nationwidechildrens). These stages are separated at specific ages due to the conditions of arterial resistance that would hinder the desired blood flow. However, during stage I, patients presenting with restricted prograde aortic flow or aortic atresia will often receive a Reverse Blalock-Taussig shunt (RBTS), sutured from the pulmonary artery to the innominate artery. The shunt is made of polytetrafluoroethylene and is usually 3.5mm or 4mm in diameter, though in some cases a 3mm shunt can be used (Honjo and Caldarone 105). It is at this stage that this paper will focus on the hemodynamic conditions of the resulting stage I Hybrid Norwood with RBTS geometry.

CHAPTER TWO: THROMBOSIS IN RBTS CAUSING STROKE INCIDENCE

The Hybrid Norwood procedure presents major complications for the patient. Mainly, the subsequent mixture of oxygenated and non-oxygenated blood strains the body, causing weakness and other physiological consequences. At the hemodynamic level, flow conditions including recirculation and stagnation caused by the artificial geometry paired with blood to shunt interaction can induce thrombosis. Thrombi particles released from the shunt location are free to travel through any of the major arteries, threatening stroke or myocardial infarction.

Along with the detailed consideration of rerouting blood flow correctly during these procedures, an obvious concern for thrombosis arises. Specifically, in the location of the RBTS, thrombosis can occur and present complications. Acute occlusion of the shunt can cause insufficient systemic flow, requiring stenting or thrombolytic therapy. With no consistent method for preventing thrombosis in the shunt, many clinicians administer doses of heparin during the use of the RBTS (Monagle 18).

There are several reasons for thrombosis occurring at the shunt. According to Chesnutt, specific levels of shear stress in blood can promote platelet aggregation (Chesnutt and Han 12). Low velocity or stagnation is also an initiator of thrombosis, as activated platelets are more likely to adhere. At the vessel wall, the flow is the lowest. Lined with endothelial cells and a plasma layer, blood vessels have natural thrombosis inhibiting factors (Shadden and Hendabadi 473). A RBTS lacks these factors and creates a higher risk of thrombosis.

Hemodynamic factors are not the only initiators of thrombosis. Foreign surfaces can promote thrombosis by activating the intrinsic pathway (May, Frauke, et al. 769). A study by Chan et al. focused on primary patency of polytetrafluoroethylene stents for treatment of venous outflow stenosis. The study found that thrombosis occurred highly on non-heparin-coated stents, having failure in less than six months. Heparin-coated stents proved to eliminate this issue (Chan et al. 652). This requires awareness that thrombosis is not only due to hemodynamic conditions, but due to foreign material as well, specifically polytetrafluoroethylene.

As thrombosis is a concern for the RBTS, one major consideration for surgical planning is the location of anastomosis. In the case of the Hybrid Norwood procedure mentioned earlier, the distal end of the shunt is sutured to the innominate artery. This opens to the common carotid artery. A danger presents itself when a possible thrombus breaks free from the shunt and embolizes to the right carotid artery, causing stroke. If thrombi were to move proximally in the ascending aorta, particles could embolize to the coronary arteries, causing myocardial infarction. These cases are a danger to the patient's life, and this paper seeks to understand the likelihood of possible thrombus embolization to specific arteries.

CHAPTER THREE: PREVIOUS WORK

Our lab group has explored the problem of thrombosis in the surrounding vasculature of the heart. As a bridge to heart transplant, mechanical assist from a Left Ventricular Assist Device (LVAD) is used in patients with failing hearts. The design of the LVAD routes blood from the left ventricle to a pump, either continuous or pulsatile, pumping blood to the ascending aorta. Thrombogenic scenarios can abound in these patients due to blood-to-foreign material contact and abnormal hemodynamic conditions of stagnation or high vorticity. As the outlet of the LVAD is sutured proximal to the cerebral vessels, thrombi can travel to the carotid and vertebral arteries and embolize. The study of our lab group was to assess by CFD which angle of anastomosis was more favorable to prevent stroke incidence. It was found that a suture of 60 degrees measured from normal to the aorta produced the most favorable results, as opposed to 30 degrees and normal (Osorio 636). Furthermore, another study by our lab group performed by Prather focused on the angle of anastomosis optimization under pulsatile flow. The results found that normal anastomosis as opposed to angled geometry was optimal for reducing cerebral artery embolization (Prather 51). These findings influence the models explored in this paper, proposing an optimal anastomosis angle exists for the case of a RBTS shunt.

The Hybrid Norwood case has also been studied and modeled by our lab group using CFD. Blood delivery was the focus of the study, determining a specific RBTS diameter optimal for ideal flow to the upper arteries. The development of such a model began with understanding the post-operative anatomy of the major arteries in the Hybrid Norwood case. A nominal model was generated using generalized geometry based on clinical data. Three separate models included a

RBTS of 3mm, 3.5mm, and 4mm in diameter. The nominal geometry can be seen below. Note the nominal model does include 90% aortic arch stenosis.

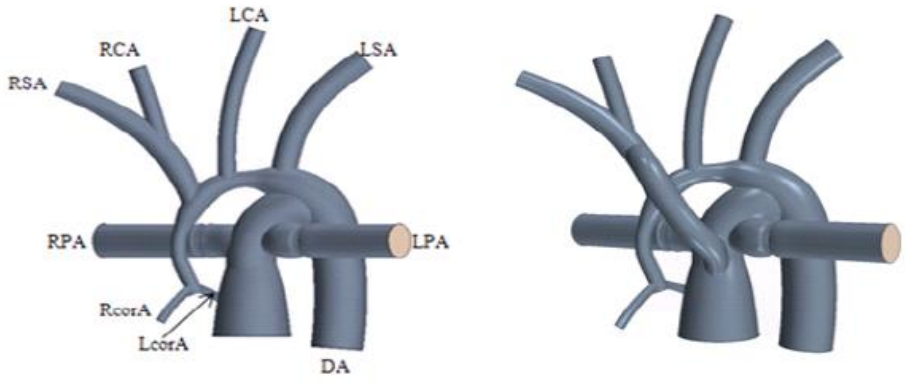

Figure 2: Nominal Anatomy Without RBTS (Left) and With RBTS (Right) (Ceballos 15)

The named outlets of the major arteries are as follows: RCA is the right carotid artery; LCA is the left carotid artery; LSA is the left subclavian artery; LPA is the left pulmonary artery; DA is the descending aorta; LcorA is the left coronary artery; RcorA is the right coronary artery; RPA is the right pulmonary artery; and RSA is the right subclavian artery. These abbreviations will be used moving forward to denote the outlets of the CFD model. This nominal model was developed to validate a patient specific model. The patient specific geometry was fabricated by compiling CT scans from a patient after stage I Hybrid Norwood and modeled using Mimics. Using 3-matic to add the RBTS of each diameter, the patient specific model was completed and can be seen below.

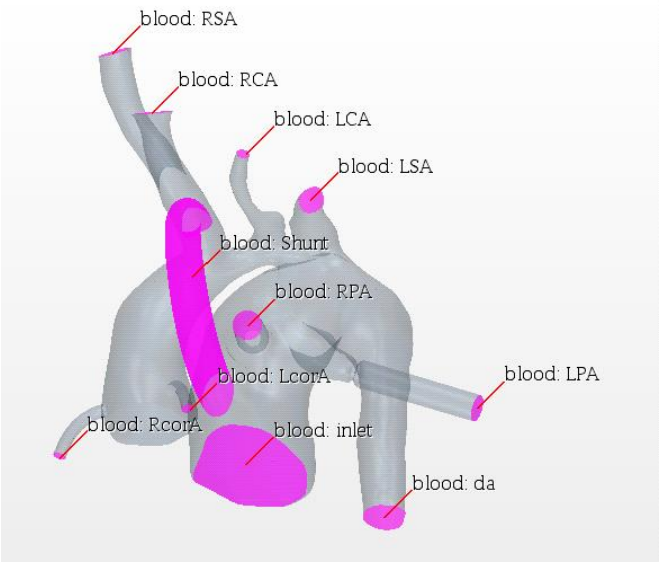

Figure 3: Patient Specific Anatomy With RBTS

The two models are comparable in scale. As each model only accounts for the geometry of the major arteries surrounding the heart, the remainder of the pulmonary and systemic flow must be accounted for to provide realistic flow fields. The solution to this was to create a Lumped Parameter Model (LPM) that treated each area in the pulmonary and systemic blood flow as elements of resistance, inductance, and capacitance relating to viscous drag, flow inertia, and vessel compliance, respectively. Diodes were comparable to the tricuspid and pulmonary valves. The resulting LPM is shown in figure 4.

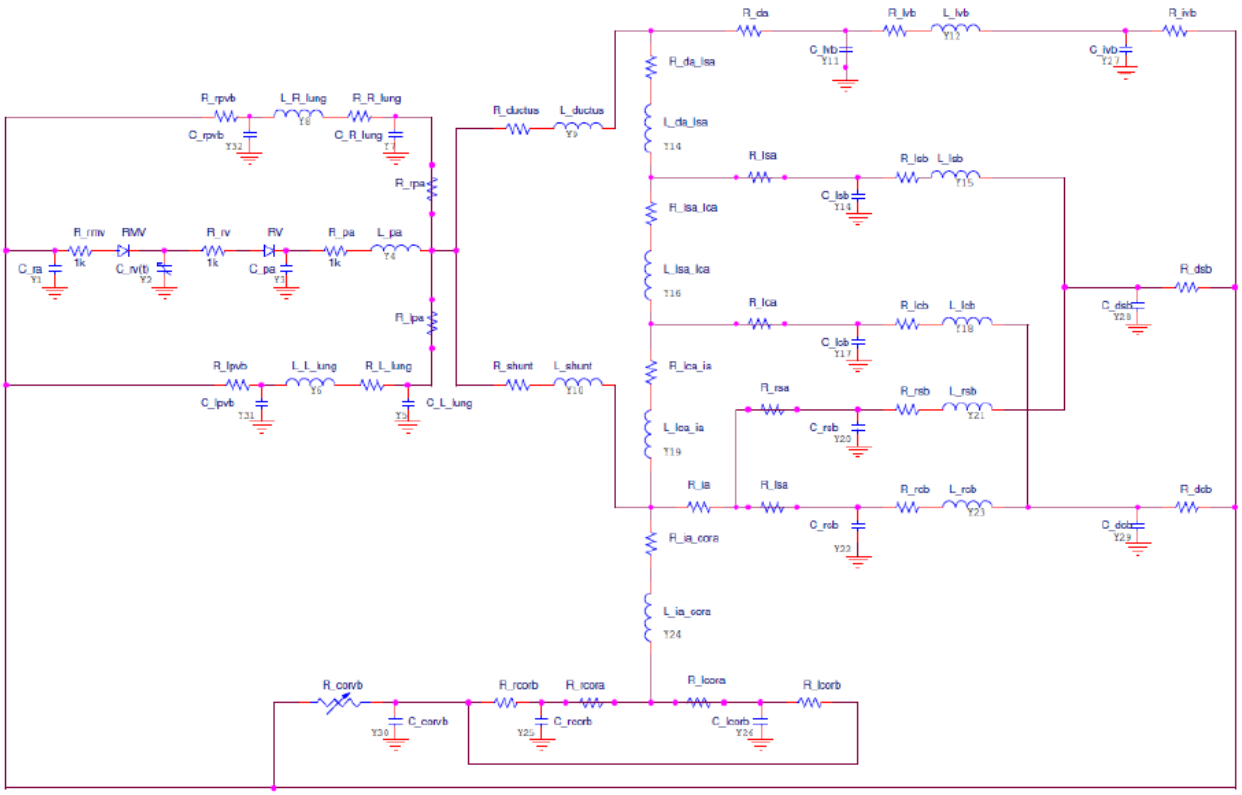

Figure 4: LPM Schematic Including RBTS (Ceballos 23)

Two governing differential equations are used for each R-L-C component:

$$\Delta p = L\frac{dQ}{dt} + RQ \qquad (1)$$

$$Q = C\frac{d(\Delta p)}{dt} \qquad (2)$$

where Δp is the pressure difference, Q is the flow rate, and t is time. Data from literature was collected to set a baseline for the values of R, L, and C. An iterative process was then used to modify these values until waveforms converged to match catheter data from literature. The right ventricle was modeled as a time dependent, pulsatile capacitor to drive the circuit. The resulting LPM consists of a 32-state variable closed loop circuit, solving ordinary differential equations

using a 4th order adaptive Ruge-Kutta solver (Ceballos 20-22). The solved values for R, L, and C are then held constant for use in all models employed in this study.

The LPM and CFD model is then coupled by first tuning the circuit to converge flow and pressures to match catheter data from literature, loading boundary conditions to the CFD model, running the CFD model to develop a flow field, updating the CFD boundaries in the circuit to equal the boundaries developed from running the CFD, running the LPM to integrate recalculated flow splits to the CFD model, and finally iterating to convergence the system of equations. Upon every iteration, flow rates change within the model. To standardize this procedure, convergence was defined when all changes in flow rates were less than 0.1 ml/min, requiring between 15 and 20 iterations in most cases. This iterative process is controlled through Star-CCM+ using a Java routine. This controls output of data from Star-CCM+, runs C-code to update boundary conditions towards convergence, loads updated data to Star-CCM+, and iterates the simulation. This loop is repeated until convergence is achieved (Ceballos 64). This process of convergence is used with 10 iterations per model discussed in the next chapter.

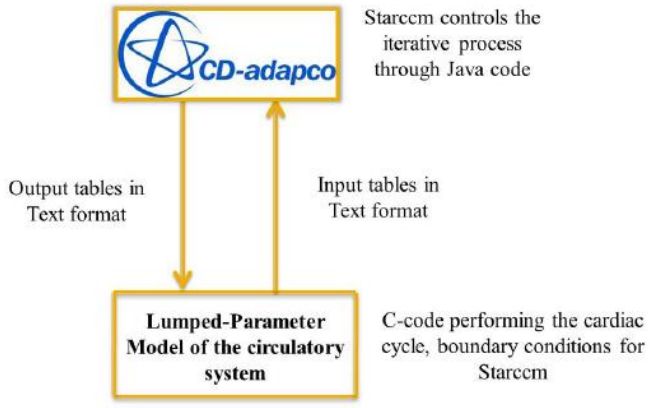

Figure 5: Schematic of Iterative Scheme (Ceballos 65)

CHAPTER FOUR: METHODS

The multiscale models were developed in Star-CCM+. The goal was to understand how manipulating the geometry of the RBTS would affect embolization rates. Models to observe were patient specific 0% and 90% aortic arch stenosis with 3mm, 3.5mm, and 4mm diameter shunts each, a nominal model with 90% aortic arch stenosis and shunt diameter of 3.5mm, and three alternate orientation options of the RBTS with 3.5mm diameter under 0% aortic arch stenosis case. As results began to populate from the first six simulations, a 3.5mm shunt seemed most preferred for critical embolization prevention. Thus, nominal model and new shunt orientation models were run using the 3.5mm shunt only.

The problem is approached as a 2-phase flow including blood-to-particle interaction, while neglecting particle-to-particle interaction. Blood is handled with a Eulerian approach as a Newtonian fluid with constant density of 1060kg/m^3 (Prather 34) under laminar flow conditions. Thrombi are modelled as solid spheres of set density of 1116.73kg/m^3 (Prather 37) and varying size (1mm and 2mm). Note that densities were found from literature in previous studies of our lab groups, and set to maintain consistency for comparisons with previous findings. Particle sizes larger than 2mm were of no interest as embolization to the shunt itself would likely occur, being out of the scope of this paper. Particle-to-wall restitution coefficients were set for perfectly elastic collisions.

The particles were tracked throughout the domain with a Lagrangian scheme, following the Lagrangian equation of motion,

$$\frac{\partial L}{\partial x_i} - \frac{d}{dt}\left(\frac{\partial L}{\partial \dot{x}_i}\right) = 0, \; i = 1,2,3 \qquad (3)$$

where L is the Lagrangian equation, the difference between kinetic and potential energy, and x is a given coordinate. Lagrangian particle tracking is described as

$$\frac{d^2\vec{r}}{dt^2} = \vec{a}(v,u) \quad (4)$$

where $\vec{r}$ is the location of the particle, $\vec{a}$ is the acceleration of the particle, $\vec{v}$ is the velocity of the particle, and $\vec{u}$ is the velocity of the fluid. The total force experienced by the particle is

$$\sum \vec{F}_{body} + \sum \vec{F}_{surface} = m_p \frac{d\vec{v}}{dt} \quad (5)$$

where m_p is the mass of the particle. This was a Lagrangian scheme based on the Maxey-Riley equation to include fluid density, particle diameter, particle relaxation time, and fluid viscosity (Maxey and Riley 884). Gravity and drag forces are included as well as added-mass effect and Saffman lift, with the vessel geometry oriented in the standing position. Thus the forces are

$$\sum \vec{F}_{body} = \vec{F}_{gravity} \quad (6)$$

$$\sum \vec{F}_{surface} = \vec{F}_{drag} + \vec{F}_{added\,mass} + \vec{F}_{saffman} \quad (7)$$

The viscous fluid model was governed by the Navier-Stokes equations for incompressible fluid

$$\nabla \cdot \vec{u} = 0 \quad and \quad \nabla \cdot \tau - \nabla p + \rho \vec{F}_{body} = \rho \left(\frac{\partial \vec{u}}{\partial t} + (\vec{u} \cdot \nabla)\vec{u} \right) \quad (8)$$

where τ is the viscous stress tensor, p is the pressure, and ρ is the density (Reddy 357). The physics continuum was modeled with Newtonian, turbulent flow with constant fluid density. The mesh

was finite volume with second order upwinding for convective derivatives. The mesh was developed as a prism layer with gap fill of 25% and element base size of 0.5mm, surface remesher, surface wrapper, and trimmer. The shunt and vessel wall surfaces were modeled as walls, while the pulmonary valve was modeled as a stagnation inlet. All other surfaces pertaining to the end of a vessel were modeled as mass flow inlets.

Each model must pass a grid independence study. As the three shunt orientation option models were developed from the beginning during this study, these models were tested by increasing and decreasing the element size by 5%. Normal element size was 0.5mm, while 0.475mm was considered for a finer mesh and 0.525mm was considered for a coarser mesh. The change in cell count between meshes did not exceed 7.52%. The flow rates and pressures throughout the models were evaluated for constant applied pressure. Between the models, the change in flow were no greater than 0.02%, with changes in pressure even lesser. The models were therefore validated for grid independence.

Option 1			Normal Element Size	0.5mm	
Normal	cell count		Fine Element Size	0.475mm	5% decrease
	612585		Coarse Element Size	0.525mm	5% increase
Fine	cell count	cell count increase	Max Flow change (ml/s)	Max Press change (mmHg)	
	658676	107.52%	0.003763254	0.012238924	
Coarse	cell count	cell count increase	Max Flow change (ml/s)	Max Press change (mmHg)	
	584468	95.41%	0.002981493	0.02918134	

Figure 6: Option 1 Grid Independence Study

Option 2				Normal Element Size	0.5mm
Normal	cell count			Fine Element Size	0.475mm 5% decrease
	616846			Coarse Element Size	0.525mm 5% increase
Fine	cell count	cell count increase		Max Flow change (ml/s)	Max Press change (mmHg)
	656480	106.43%		0.004276	0.036433
Coarse	cell count	cell count increase		Max Flow change (ml/s)	Max Press change (mmHg)
	584077	94.69%		0.010608	0.004372

Figure 7: Option 2 Grid Independence Study

Option 3				Normal Element Size	0.5mm
Normal	cell count			Fine Element Size	0.475mm 5% decrease
	579635			Coarse Element Size	0.525mm 5% increase
Fine	cell count	cell count increase		Max Flow change (ml/s)	Max Press change (mmHg)
	621193	107.17%		0.004426433	0.032191
Coarse	cell count	cell count increase		Max Flow change (ml/s)	Max Press change (mmHg)
	559175	96.47%		0.003752502	0.029246

Figure 8: Option 3 Grid Independence Study

Due to the nature of flow in the shunt, three separate release locations are employed in the conduit: (1) proximal, (2) medial, and (3) distal to the RBTS-pulmonary root anastomosis. The initial velocity of these particles was set as 0m/s. Each particle released was counted with its specific size and release location, providing data on where particles are prone to travel based on release location.

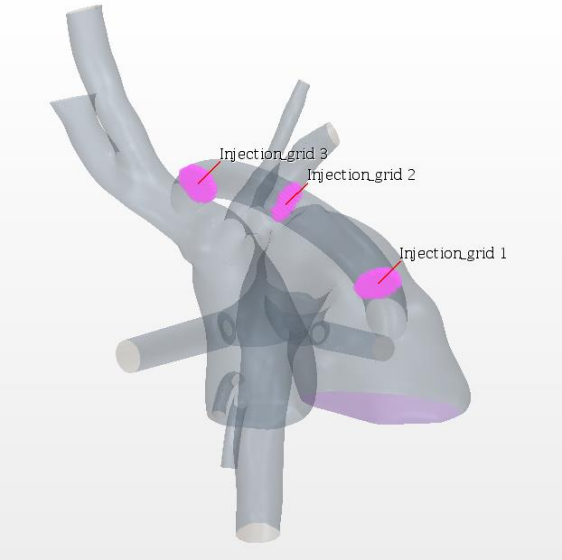

Figure 9: Particle Injection Plane Location (1=Proximal, 2=Medial, 3=Distal)

For purely statistical purposes, particle interactions are limited to particle-to-wall and particle-to-flow interactions. Particle velocities are plotted real time and particle counters are set at each boundary outlet to determine when and where particles leave the domain during several heart cycles. Each model was set to output approximately 300 particles of both diameters over three heart cycles. The models were run once to develop the flow field and particle presence, then run six times to collect data. The average and standard deviation was calculated from the results for each particle size and release location per model.

Statistical significance was determined by the Chi-Square Test

$$\chi^2 = \sum \frac{(O-E)^2}{E} \qquad (9)$$

where O is the observed data, and E is the expected data. A specific procedure was performed to determine the Chi-Square value of the resulting data sets. This test involves summing the rows and

columns for the given data set, and summing the sums of the rows and columns. Expected values are set for each data point by multiplying that data point's column sum by its row sum, then dividing by the sum of the sums of the rows and sums of the columns. The Chi-Square calculation value for a specific data point is the observed value less the expected value squared, divided by the expected value. Once the Chi-Square calculation data is collected into a table relative to the original data set, the sum of the sums of the rows and the sums of the columns outputs the Chi-Square value for the original data set. This value must exceed the values in the table below per the degrees of freedom and desired confidence level.

Table 1: Chi-Square Probabilities (Penn State)

df	$\chi^2_{.995}$	$\chi^2_{.990}$	$\chi^2_{.975}$	$\chi^2_{.950}$	$\chi^2_{.900}$	$\chi^2_{.100}$	$\chi^2_{.050}$	$\chi^2_{.025}$	$\chi^2_{.010}$	$\chi^2_{.005}$
1	0.000	0.000	0.001	0.004	0.016	2.706	3.841	5.024	6.635	7.879
2	0.010	0.020	0.051	0.103	0.211	4.605	5.991	7.378	9.210	10.597
3	0.072	0.115	0.216	0.352	0.584	6.251	7.815	9.348	11.345	12.838
4	0.207	0.297	0.484	0.711	1.064	7.779	9.488	11.143	13.277	14.860
5	0.412	0.554	0.831	1.145	1.610	9.236	11.070	12.833	15.086	16.750
6	0.676	0.872	1.237	1.635	2.204	10.645	12.592	14.449	16.812	18.548
7	0.989	1.239	1.690	2.167	2.833	12.017	14.067	16.013	18.475	20.278
8	1.344	1.646	2.180	2.733	3.490	13.362	15.507	17.535	20.090	21.955
9	1.735	2.088	2.700	3.325	4.168	14.684	16.919	19.023	21.666	23.589
10	2.156	2.558	3.247	3.940	4.865	15.987	18.307	20.483	23.209	25.188
11	2.603	3.053	3.816	4.575	5.578	17.275	19.675	21.920	24.725	26.757
12	3.074	3.571	4.404	5.226	6.304	18.549	21.026	23.337	26.217	28.300
13	3.565	4.107	5.009	5.892	7.042	19.812	22.362	24.736	27.688	29.819
14	4.075	4.660	5.629	6.571	7.790	21.064	23.685	26.119	29.141	31.319
15	4.601	5.229	6.262	7.261	8.547	22.307	24.996	27.488	30.578	32.801
16	5.142	5.812	6.908	7.962	9.312	23.542	26.296	28.845	32.000	34.267
17	5.697	6.408	7.564	8.672	10.085	24.769	27.587	30.191	33.409	35.718
18	6.265	7.015	8.231	9.390	10.865	25.989	28.869	31.526	34.805	37.156
19	6.844	7.633	8.907	10.117	11.651	27.204	30.144	32.852	36.191	38.582
20	7.434	8.260	9.591	10.851	12.443	28.412	31.410	34.170	37.566	39.997
21	8.034	8.897	10.283	11.591	13.240	29.615	32.671	35.479	38.932	41.401
22	8.643	9.542	10.982	12.338	14.041	30.813	33.924	36.781	40.289	42.796
23	9.260	10.196	11.689	13.091	14.848	32.007	35.172	38.076	41.638	44.181
24	9.886	10.856	12.401	13.848	15.659	33.196	36.415	39.364	42.980	45.559
25	10.520	11.524	13.120	14.611	16.473	34.382	37.652	40.646	44.314	46.928
26	11.160	12.198	13.844	15.379	17.292	35.563	38.885	41.923	45.642	48.290
27	11.808	12.879	14.573	16.151	18.114	36.741	40.113	43.195	46.963	49.645
28	12.461	13.565	15.308	16.928	18.939	37.916	41.337	44.461	48.278	50.993
29	13.121	14.256	16.047	17.708	19.768	39.087	42.557	45.722	49.588	52.336
30	13.787	14.953	16.791	18.493	20.599	40.256	43.773	46.979	50.892	53.672
40	20.707	22.164	24.433	26.509	29.051	51.805	55.758	59.342	63.691	66.766
50	27.991	29.707	32.357	34.764	37.689	63.167	67.505	71.420	76.154	79.490
60	35.534	37.485	40.482	43.188	46.459	74.397	79.082	83.298	88.379	91.952
70	43.275	45.442	48.758	51.739	55.329	85.527	90.531	95.023	100.425	104.215
80	51.172	53.540	57.153	60.391	64.278	96.578	101.879	106.629	112.329	116.321
90	59.196	61.754	65.647	69.126	73.291	107.565	113.145	118.136	124.116	128.299
100	67.328	70.065	74.222	77.929	82.358	118.498	124.342	129.561	135.807	140.169

See APPENDIX B for Chi-Square sample calculation. All data sets passed α of 0.005 at four degrees of freedom. The degrees of freedom were shunt diameter, particle diameter, particle release location, and exit boundary.

CHAPTER FIVE: STATISTICAL RESULTS AND DISCUSSION

Three shunt sizes are investigated: 3mm, 3.5mm, and 4mm in diameter. Two different particle sizes are used in each case: 1mm and 2mm in diameter. The simulations were run for the duration of three heart cycles. Monitors tracked boundary exit of each particle with respect to its size and release location. Data tables were populated and averaged over all release locations. See APPENDIX B for complete data including variance. Note that the inlet boundary refers to the pulmonary valve.

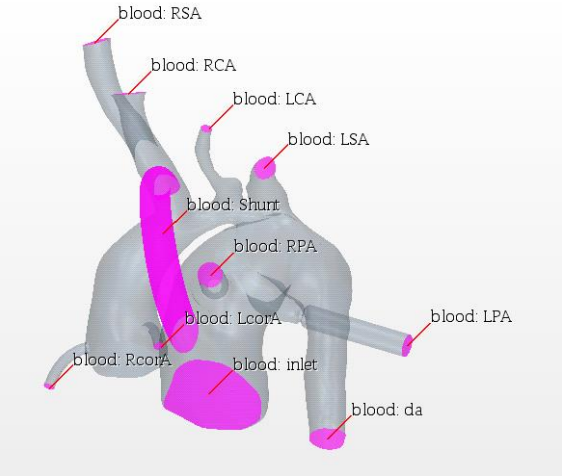

Figure 10: Boundary Nomenclature of Multiscale Model

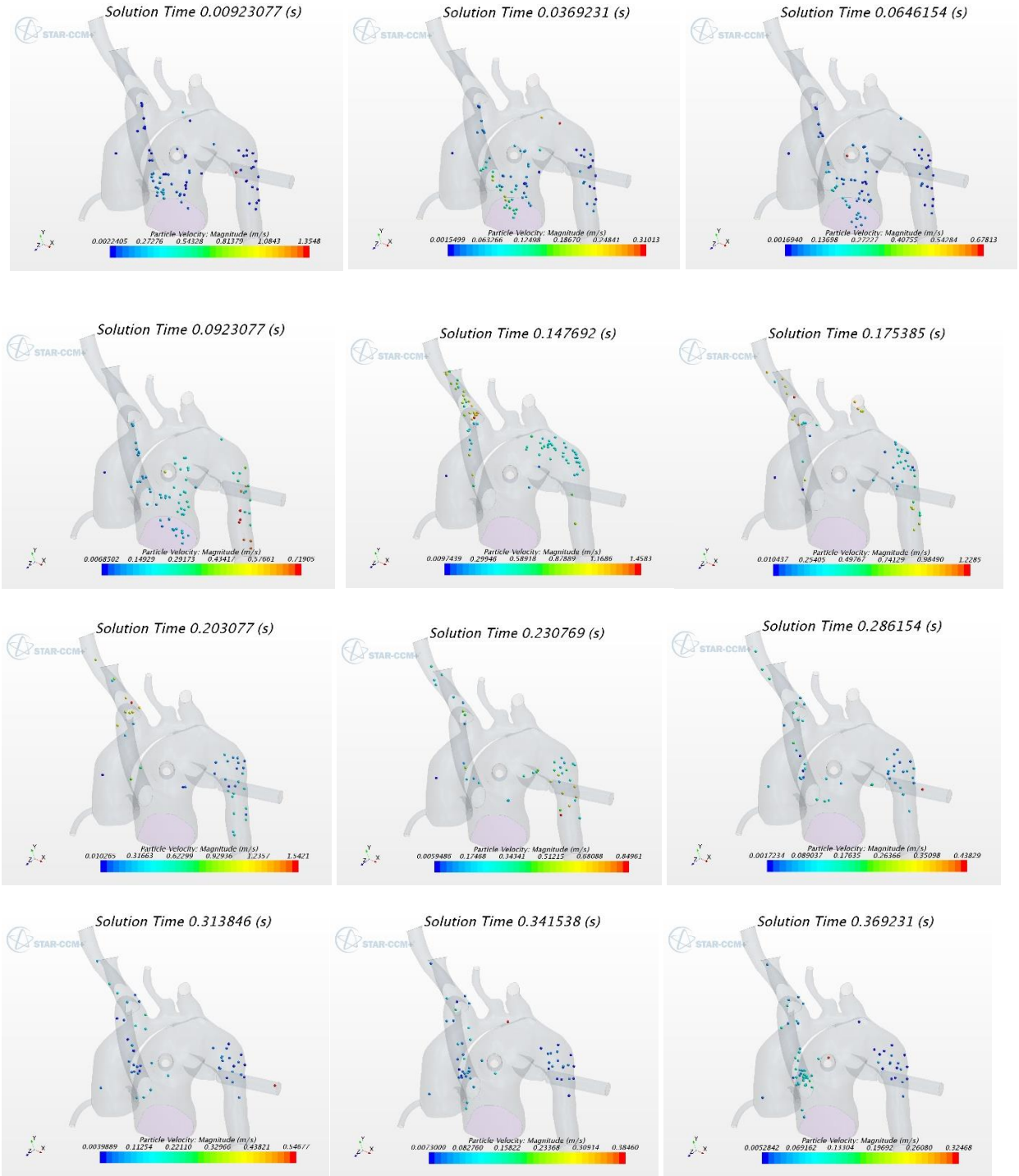

Figure 11: Patient Specific, No Stenosis, 3.5mm RBTS Particle Tracking

Table 2: Embolization Rates for Various Shunt/Particle Size (Patient Specific, No Stenosis)

Results		RSA	RCA	LCA	LSA	RcorA	LcorA	RPA	LPA	DA	inlet
3mmBT Shunt	1mm Particles	13.80%	54.24%	4.89%	11.25%	0.05%	0.74%	2.13%	2.69%	9.80%	0.42%
	2mm Particles	15.96%	38.86%	3.73%	5.21%	0.00%	0.49%	0.51%	3.52%	30.46%	1.25%
3.5mmBT Shunt	1mm Particles	18.98%	49.46%	1.81%	5.13%	0.08%	1.97%	1.15%	4.45%	15.47%	1.49%
	2mm Particles	17.00%	41.67%	2.41%	4.83%	0.00%	0.09%	0.96%	4.61%	28.01%	0.41%
4mmBT Shunt	1mm Particles	22.45%	47.38%	2.52%	6.10%	0.20%	2.73%	1.02%	3.85%	13.60%	0.16%
	2mm Particles	18.69%	42.87%	2.29%	4.00%	0.00%	0.00%	0.90%	4.69%	26.30%	0.26%

For the patient specific, no stenosis case, embolization rates are significantly high to the RCA across all shunt sizes. Embolization to the LCA is least for the 3.5mm RBTS and LcorA embolization is favorable over the 4mm RBTS. The coronary arteries experience higher embolization rates for 1mm particles over 2mm particles. A 2mm particle would have higher mass, and thus, a higher stokes number. It is reasonable to assume that a lower stokes number particle would be more likely to follow streamlines downward towards the coronary arteries instead of continuing in the direction of the shunt anastomosis as a heavier particle would. There is an inverse relationship between embolization rates to the RCA for 1mm and 2mm particles with increasing shunt diameter. As the shunt increases, 1mm particles decrease in embolization, while 2mm particles increase in embolization. The flow produced from a larger shunt must compete with flow entering the aortic arch from the pulmonary trunk. This mixture of flow separates particles of different mass, sending particles with lower Stokes number along the streamlines. There is likely a specific mass, or diameter in this case, of particle which does not change its embolization to the

RCA as a function of shunt diameter. What these results do show is that particles small enough to fit within the vessels surrounding the heart can take completely different paths based on their mass.

The following table and figure display the critical embolization risks for the 0% stenosis case.

Table 3: Critical Embolization Rates – 0% Stenosis

	Stroke	Myocardial Infarction
3mmBT Shunt	50.86%	0.64%
3.5mmBT Shunt	47.68%	1.07%
4mmBT Shunt	47.53%	1.46%

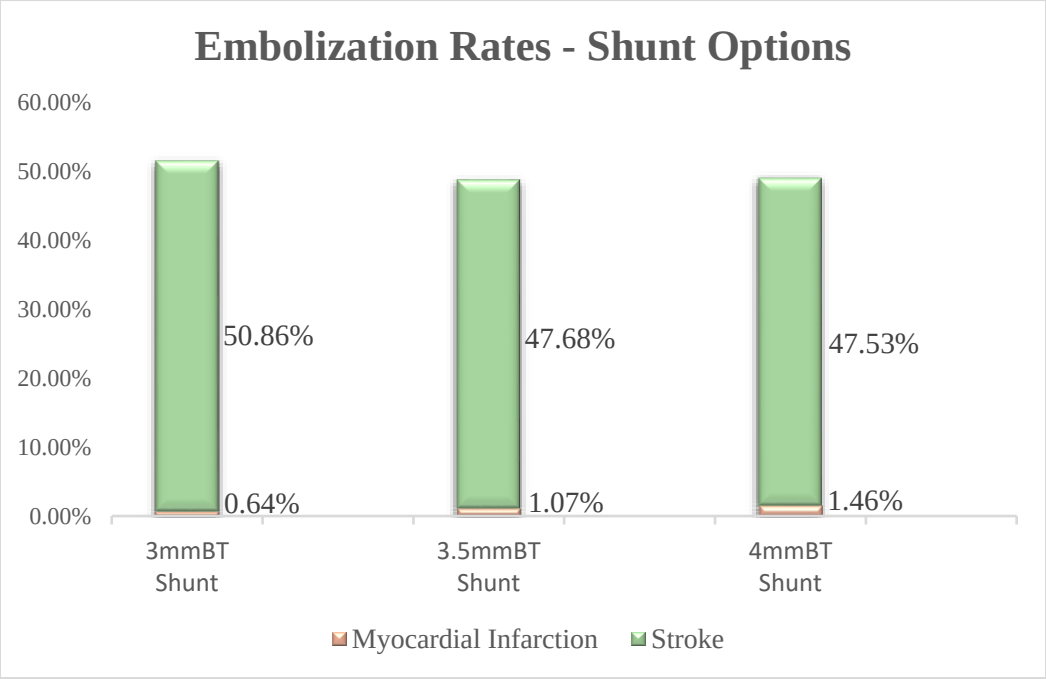

Figure 12: Critical Embolization Rates – 0% Stenosis

Overall, the 0% stenosis case involves high embolization to the carotid arteries. The 3.5mm shunt reduces stroke risk, while maintaining low coronary embolization. In general, the rates do not vary significantly between the three shunt sizes, and there is an inverse relationship of stroke risk to myocardial infarction risk.

Table 4: Embolization Rates for Various Shunt/Particle Size (Patient Specific, 90% Stenosis)

Results		RSA	RCA	LCA	LSA	RcorA	LcorA	RPA	LPA	DA	inlet
3mmBT Shunt	1mm Particles	14.62%	15.25%	5.33%	1.31%	2.85%	1.01%	0.33%	3.17%	14.34%	41.79%
	2mm Particles	8.83%	10.15%	9.32%	1.81%	2.78%	1.36%	2.51%	12.61%	19.22%	31.40%
3.5mmBT Shunt	1mm Particles	12.53%	27.11%	8.38%	7.36%	3.94%	0.85%	1.36%	3.24%	21.49%	13.74%
	2mm Particles	8.23%	12.46%	12.64%	4.44%	3.47%	2.20%	4.39%	9.16%	26.14%	16.87%
4mmBT Shunt	1mm Particles	11.81%	30.44%	10.57%	8.03%	3.42%	0.71%	1.23%	3.65%	18.66%	11.47%
	2mm Particles	7.05%	15.30%	11.53%	3.87%	4.60%	3.25%	3.84%	9.48%	24.25%	16.81%

For the patient specific, 90% aortic arch stenosis, embolization rates are much higher for the coronary arteries. The carotid arteries along with the subclavian arteries experience less embolization to the no-stenosis case, while the inlet, or pulmonary valve showed higher embolization. For this case, the 3mm RBTS is most favorable for critical arteries, though the pulmonary valve experiences significant embolization. As the shunt is smaller, resistance is expected to be higher. Particles may not completely exit the shunt before retro flow occurs and pulls the particles towards the pulmonary valve. In this case of stenosis, embolization of 1mm and 2mm particles increase embolization to the RCA with increasing shunt diameter. This is not the inverse relationship seen in the 0% stenosis case, and may be due to the lack of flow through the

aortic arch. The following table and figure display critical embolization rates for each shunt diameter in the 90% stenosis case.

Table 5: Critical Embolization Rates – 90% Stenosis

	Stroke	Myocardial Infarction
3mmBT Shunt	20.02%	4.00%
3.5mmBT Shunt	30.30%	5.23%
4mmBT Shunt	33.92%	5.99%

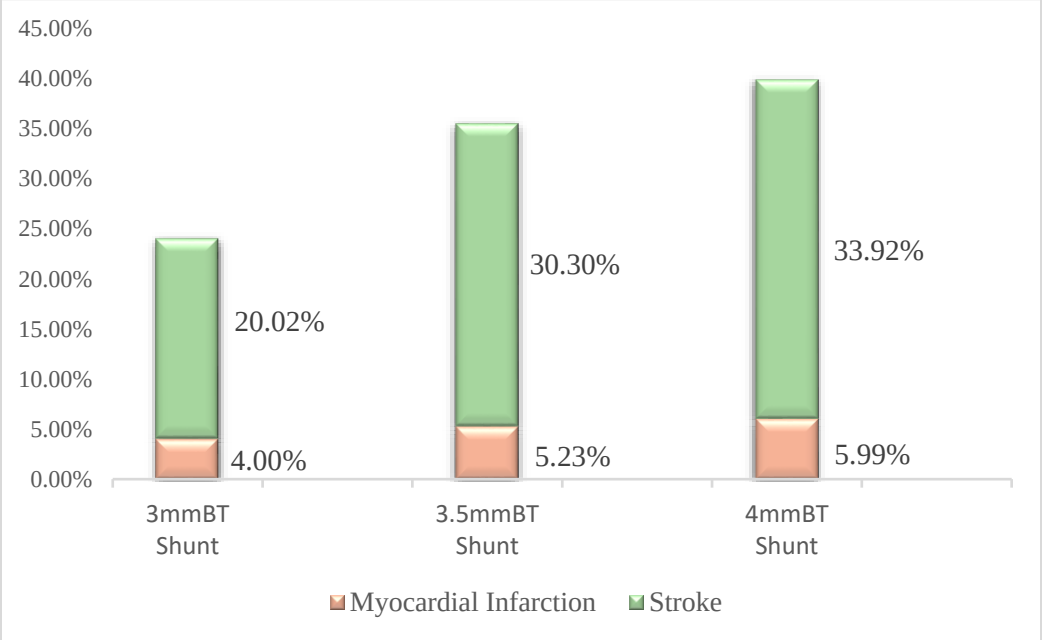

Figure 13: Critical Embolization Rates – 90% Stenosis

The 90% stenosis case observes lower embolization to the carotid arteries than the case of no stenosis. Higher embolization to the coronaries is also a difference with stenosis. In general, with 90% stenosis, the 3mm shunt reduces critical embolization in both carotid and coronary arteries.

Between the two stenosis cases, the streamlines in the ascending aorta are quite different (see figure below). The 0% stenosis case shows smoother streamlines, while the 90% stenosis case displays more vortices. As the stenosis would constrict flow to evenly split from the shunt to the coronaries, carotids, and descending aorta, blood circulates within the ascending aorta and particles seem to exist in that space longer, lending to a higher probability of embolization to the coronaries.

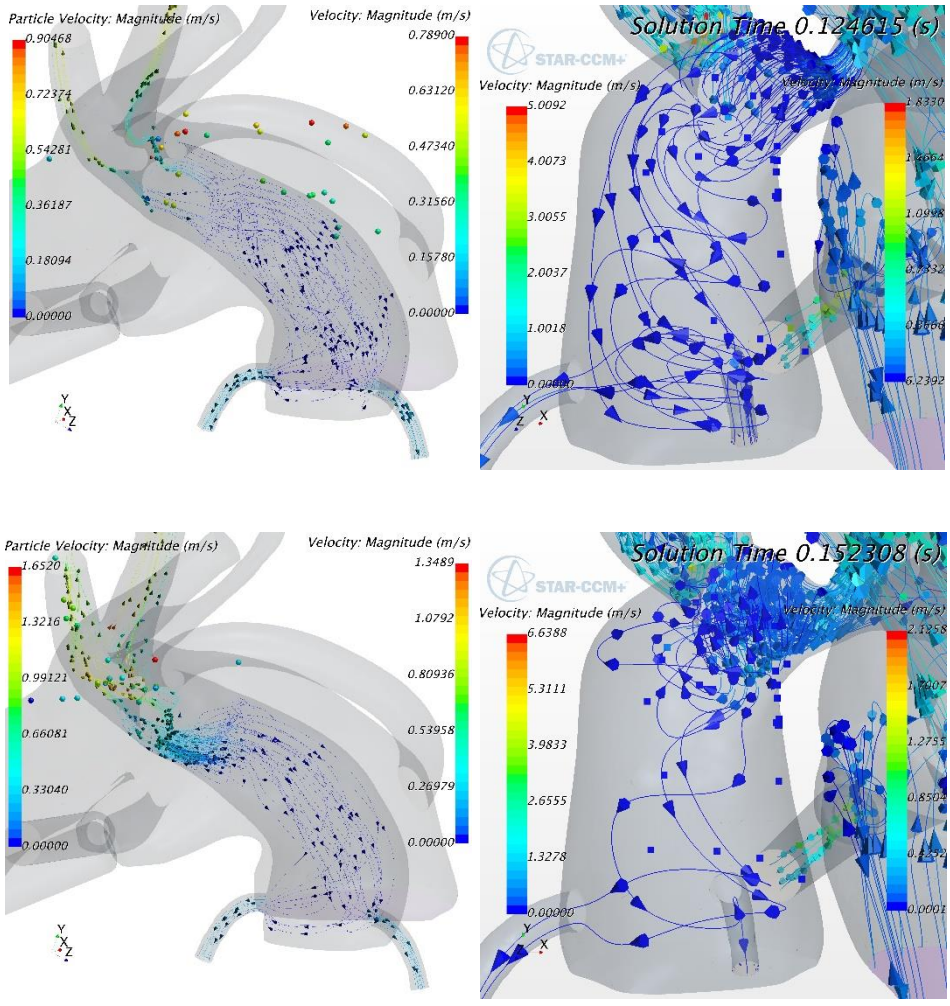

Figure 14: No Stenosis (Left) Vs. 90% Stenosis (Right) Streamlines in Ascending Aorta

One important comparison to make between the two stenosis cases is the RCA embolization. In the 0% stenosis case, RCA embolization rates are significantly high. These drastic levels are not seen with 90% stenosis. When the aortic arch is constricted due to stenosis, a majority of flow to the common carotid and left carotid artery must come from the shunt. This causes higher flow rate in the shunt, and more distribution of particles to these arteries. When the aortic arch is free to provide flow, flow velocity is decreased in the shunt. This decrease in flow promotes a prothrombotic hemodynamic environment. Particles originating within the shunt are also forced into the common carotid artery from opposing aortic arch flow. Thus, a patient presenting with no aortic arch stenosis has a greater risk of embolization to the RCA fueled by two factors. Surgeons should be aware of this finding, as it can suggest that a patient with no aortic arch stenosis should not receive a RBTS unless absolutely necessary.

Table 6: Embolization Rates for 3.5mm Shunt Size and Various Particle Size (Nominal, 90% Stenosis)

Results		RSA	RCA	LCA	LSA	RcorA	LcorA	RPA	LPA	DA	inlet
3.5mmBT Shunt	1mm Particles	16.96%	9.71%	7.69%	3.65%	2.03%	3.80%	18.54%	14.21%	23.29%	0.13%
	2mm Particles	6.38%	8.60%	13.31%	3.23%	2.91%	5.56%	23.67%	9.51%	25.02%	1.81%

The 90% stenosis nominal model was run for the 3.5mm RBTS to compare findings from the 90% stenosis patient specific model. Trends in embolization to the coronary arteries and carotid arteries are consistent between the nominal and patient specific cases. However, large variation in data is shown in the pulmonary arteries and pulmonary valve. Variation itself supports the fact that this method must be applied to the specific geometry of the patient in question. Possible results

can be implied from similar geometry. But for the purpose of surgical planning, exact geometry should be used. Below displays the critical embolization risks for the nominal geometry.

Table 7: Critical Embolization Rates – Nominal Geometry

	Stroke	Myocardial Infarction
3.5mmBT Shunt	19.65%	7.15%

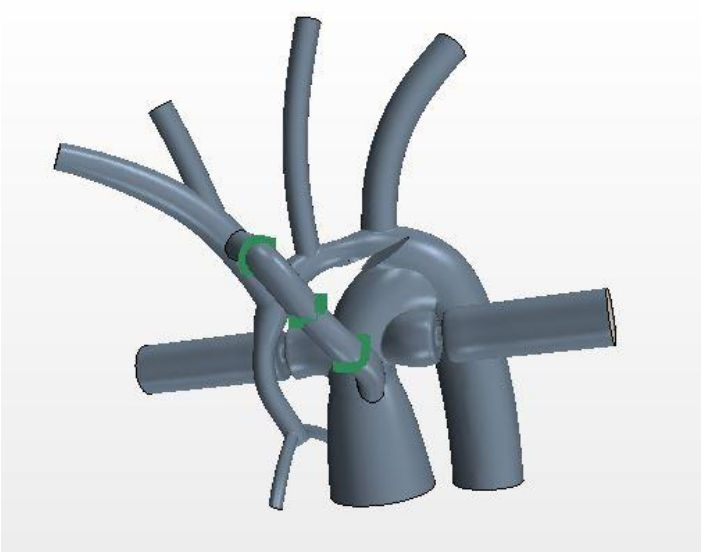

Figure 15: 90% Stenosis Nominal Geometry with Three Particle Injection Planes (In Green)

After obtaining the results from the no stenosis, 90% stenosis, and 90% stenosis nominal cases, three differing shunt orientations were modeled to attempt at reducing embolization rates to the carotid arteries. The three attempts were to increase angle of anastomosis at the innominate artery, move the shunt out of plane to have an outlet normal in line with the aortic arch, and to move the anastomosis proximal on the ascending aorta. The shunt diameter was held constant at 3.5mm between the three options. The generated models are as follows.

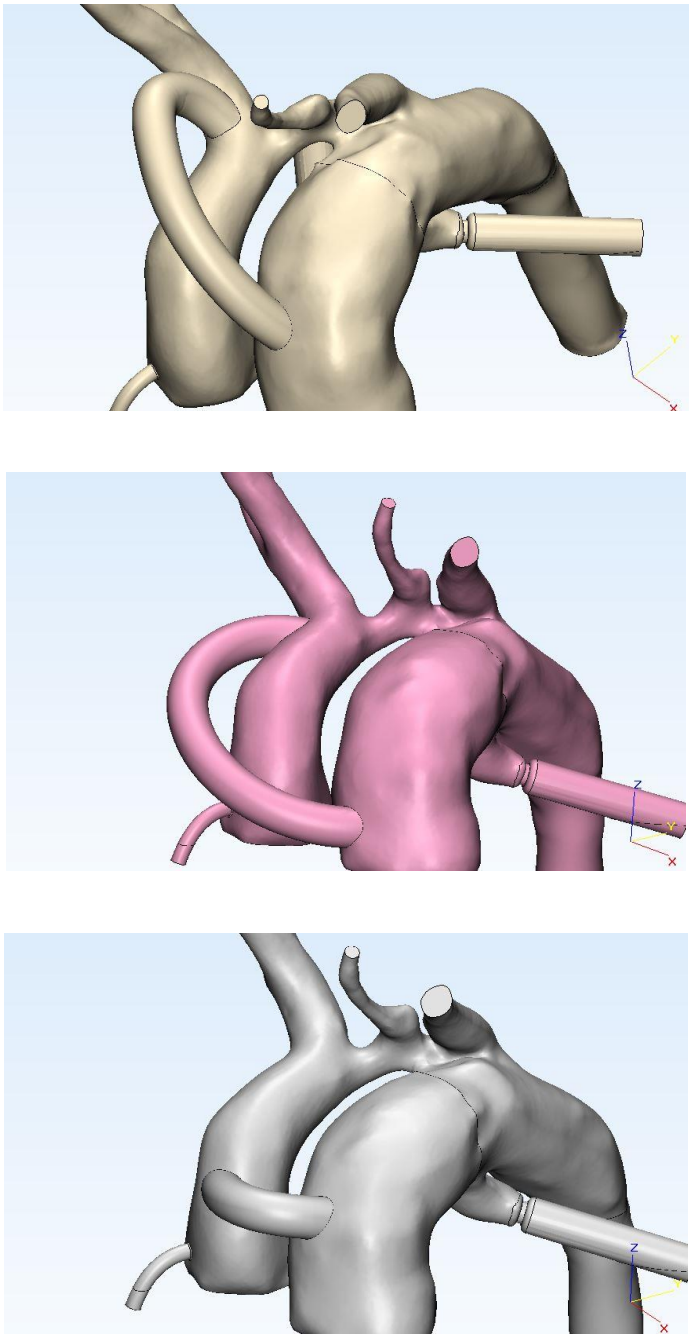

Figure 16: New Shunt Geometries Including Option 1 (Top), Option 2 (Middle), and Option 3 (Bottom)

Table 8: Embolization Rates for 3.5mmBT Shunt and Various Particle Size and Geometry Option (Patient Specific, No Stenosis)

Results		RSA	RCA	LCA	LSA	RcorA	LcorA	RPA	LPA	DA	inlet
OPT 1	1mm Particles	13.94%	42.57%	8.76%	14.03%	0.23%	1.05%	2.17%	2.82%	14.33%	0.09%
	2mm Particles	19.94%	32.51%	12.45%	3.65%	0.46%	2.77%	6.89%	5.22%	11.84%	4.28%
OPT 2	1mm Particles	17.73%	35.01%	6.53%	5.59%	0.15%	1.56%	2.41%	5.18%	17.27%	8.57%
	2mm Particles	26.47%	18.66%	8.64%	2.47%	0.55%	1.67%	2.71%	3.53%	14.00%	21.29%
OPT 3	1mm Particles	11.17%	10.74%	4.64%	9.61%	0.68%	3.23%	15.95%	15.81%	27.28%	0.88%
	2mm Particles	8.23%	10.99%	8.33%	3.09%	1.12%	8.12%	20.47%	16.39%	20.38%	2.89%

The results for all three options are indicative that shunt placement is critical in surgical planning. Option 1 presents benefits in embolization rates to the right carotid artery over the original geometry. The increased angle of anastomosis was successful in directing particles away from the right carotid artery. However, the right subclavian artery experienced more embolization. The increased angle of anastomosis causes the flow to impact directly into the innominate artery wall and create a highly vorticial environment. This would cause particles to change direction and move towards the common carotid artery. This option was initially intended to point particle flow away from the right carotid artery, and it did just that. However, the flow of particles still exists in the common carotid artery, though directed towards a less life threatening path. The left carotid artery suffered more embolization, which would be expected if particles would be diverted from the right carotid artery and move towards the aortic arch. This effect is seen in all three options, but option 2 and 3 show significant right carotid artery embolization prevention, with option 3 at the greatest. Most particles in these last two options are in the end diverted towards the pulmonary

arteries and descending aorta. Embolization rates to the coronaries increase substantially from the original geometry in all cases. Option 3 presents a major coronary embolization issue. This is understandable for option 3 as the outlet of the shunt is closer to the coronary arteries. As mentioned before, option 3 decreases embolization to the RCA significantly. This is likely due to how the particles behave when first injected. Starting at a velocity of 0m/s, the particles take time to accelerate and follow the streamlines, with heavier particles increasing that time. Since the shunt in option 3 is sutured so far away from the RCA, particles seem to accelerate with enough time to follow the flow field away from the RCA. Additionally, in a practical setting, a shunt of such short length would reduce chances of thrombosis as there is less blood-to-foreign surface contact. One should note that the patient specific model is in fact specific to the patient. Other patient geometries may not be as suitable for any one of these three shunt placements. Additionally, in many cases, ascending aortic atresia can reduce the surface area available for suturing the RBTS. If the ascending aorta is small enough, option 3 may not even be possible. The following table and graph display the associated risks of stroke or myocardial infarction between the three shunt placement options.

Table 9: Critical Embolization Rates – Shunt Placement Options

	Stroke	Myocardial Infarction
OPT 1	48.15%	2.26%
OPT 2	34.42%	1.96%
OPT 3	17.35%	6.58%

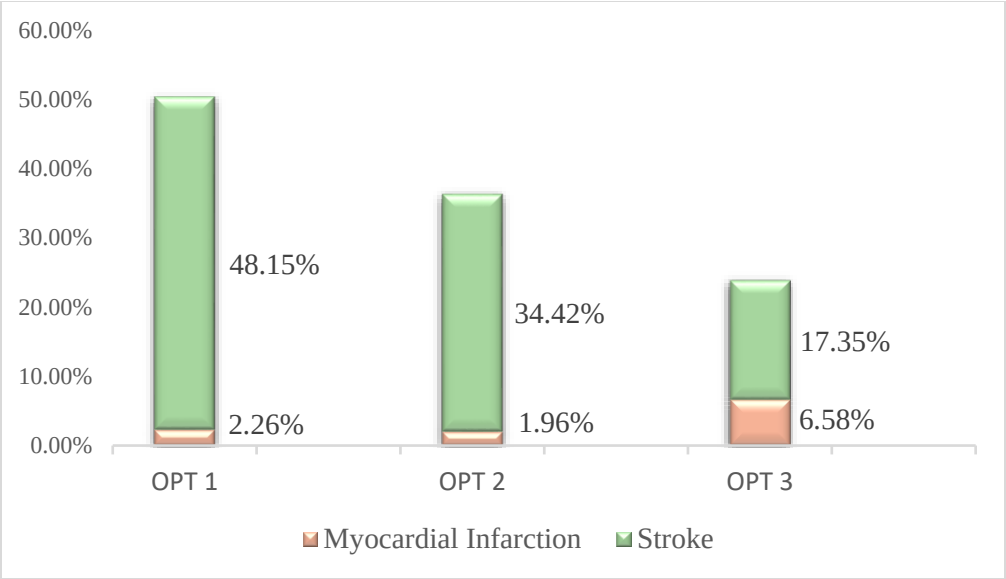

Figure 17: Critical Embolization Rates – Shunt Placement Options

In general, option 3 reduces stroke risk significantly. However, myocardial infarction risk is approximately three times higher when compared to the other two options. Option 2 reduces carotid artery embolization significantly while reducing coronary embolization to the lowest rate among the three options.

The results shown above for varying shunt size and placement prove that surgical planning can benefit from patient specific CFD models. Depending on the patient geometry, a specific shunt diameter and placement can be chosen to minimize stroke or myocardial infarction risk. As seen in this case, a 3.5mm RBTS in placement option 2 reduces stroke risk while managing coronary embolism, and is still possible in the case of severe ascending aortic atresia.

CHAPTER SIX: FUTURE WORK

In every model employed in this study, particles are randomly released at arbitrary times during the heart cycle. In reality, a thrombus may require a specific amount of shear to separate from the shunt wall, occurring during systole and not during diastole. As such, newer models may track particle release time and create statistics based on time release. The results may reveal interesting trends in embolization rates. Alternatively, if data were collected on hemodynamic conditions required to separate thrombi from the shunt wall, the simulation could incorporate such a range of values to only release a particle when a specific point is experiencing pressure above the threshold.

The particles in this study were modeled as simple spheres with a coefficient of restitution of 1 for particle-to-wall interaction. These are simply not the true characteristics of thrombi, as their makeup is gelatinous and deformable. Further studies must be done to quantify the physical properties of thrombi as they relate to restitution and shape. Incorporating such data into the models used in this paper may provide more realistic results.

CHAPTER SEVEN: CONCLUSION

This study presents CFD as a viable and effective tool in determining surgical plans. In the patient geometry of this study, an optimal shunt size of 3.5mm in diameter could be determined for reducing cerebral thromboembolization in the zero-stenosis case, while the 90% stenosis case requires a 3mm shunt size. In both stenosis cases, the 3mm shunt reduces embolization to the coronaries. A shunt with increased angle of anastomosis reduced embolization to the right coronary artery, however other critical arteries suffered higher embolization. A shunt in plane with the aortic arch reduced embolization to the right carotid artery, while maintaining low embolization to the left carotid and coronary arteries. A shunt with anastomosis proximal to the innominate artery prevents common carotid embolization in general, though it increases coronary embolization significantly. These results suggest, in general, 3-3.5mm shunts at shorter lengths with anastomosis proximal to the innominate artery seem to be best practice in the Hybrid Norwood procedure. In the case of ascending aortic atresia, a 3-3.5mm shunt in plane with the aortic arch would still minimize potential life threatening embolization. A RBTS may even be determined to be a dangerous option for stage I palliation for a patient presenting with minimal aortic arch stenosis. In summary, a surgeon can utilize this method to numerically justify a surgical plan for reducing stroke incidence or myocardial infarction given the geometry of the patient of concern. Every decision made by the surgeon can have severe consequences, so it is paramount that as much information as possible is at his or her disposal. As the Hybrid Norwood procedure is used often in HLHS, understanding embolization rates associated with the RBTS geometry of concern will better equip physicians to administer this life changing procedure and ensure higher success rates.

APPENDIX A: DA PRESSURE PLOT

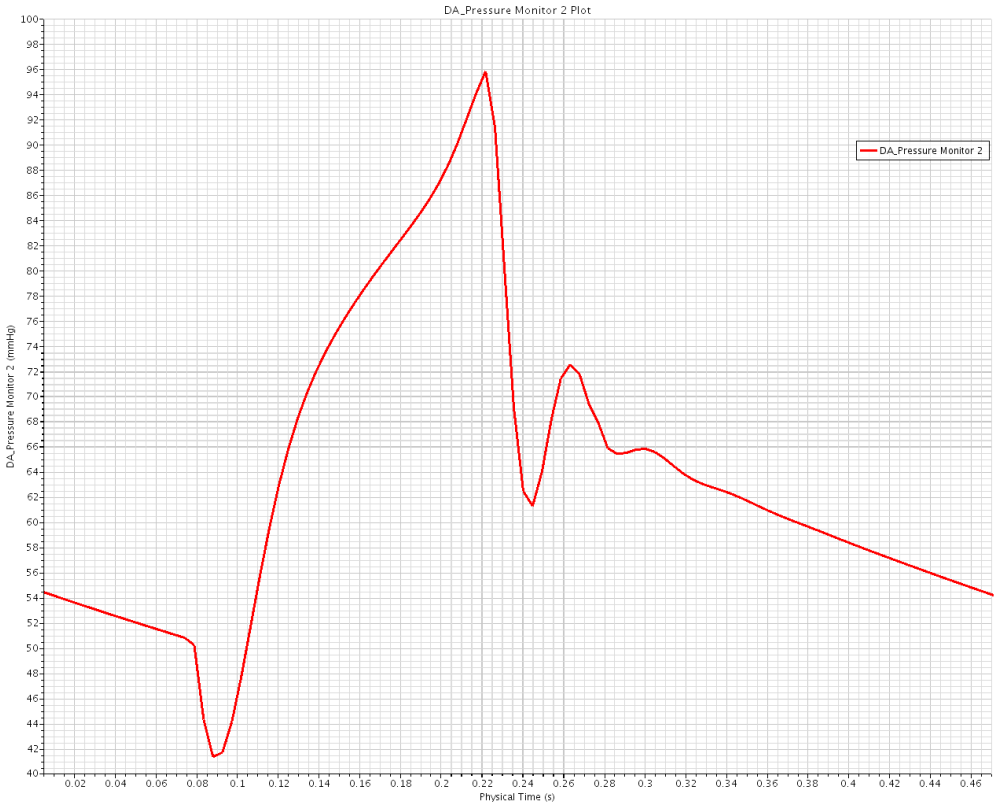

Figure 18: Pressure Plot of Descending Aorta Boundary During One Heart Cycle

APPENDIX B: IN-DEPTH STATISTICAL ANALYSIS

Table 10: Embolization Rates for Various Shunt/Particle Size (Patient Specific, No Stenosis) Including Variance

Results w/ Variance			RSA	RCA	LCA	LSA	RcorA	LcorA	RPA	LPA	DA	inlet
3mmBT Shunt	1mm Particles	Proximal	8.31±0.48%	36.07±3.32%	8.20±3.71%	22.31±5.60%	0.08±0.17%	0.87±0.38%	0.98±1.12%	3.47±1.63%	18.72±7.85%	1.00±0.90%
		Medial	9.33±2.71%	65.38±7.31%	4.44±2.13%	9.37±3.03%	0.00±0.00%	0.96±1.13%	1.23±1.12%	2.37±2.15%	6.66±3.97%	0.26±0.58%
		Distal	23.76±2.26%	61.27±4.20%	2.01±0.40%	2.06±0.97%	0.08±0.18%	0.37±0.54%	4.19±1.88%	2.23±0.56%	4.02±1.35%	0.00±0.00%
	2mm Particles	Proximal	9.24±0.97%	25.80±3.13%	4.19±0.94%	8.11±1.39%	0.00±0.00%	0.68±0.30%	0.14±0.19%	4.24±1.35%	45.31±1.73%	2.29±0.98%
		Medial	12.67±4.12%	42.78±6.78%	4.21±1.77%	5.38±1.82%	0.00±0.00%	0.00±0.00%	0.74±0.76%	3.62±2.11%	29.54±7.88%	1.06±1.18%
		Distal	25.97±1.61%	47.99±3.35%	2.79±0.28%	2.14±0.72%	0.00±0.00%	0.81±0.37%	0.64±0.40%	2.70±1.32%	16.54±2.34%	0.41±0.32%
3.5mmBT Shunt	1mm Particles	Proximal	10.32±1.02%	31.91±3.82%	2.59±0.91%	9.48±1.46%	0.00±0.00%	1.06±0.09%	1.67±0.54%	8.07±1.01%	32.05±4.15%	2.85±0.68%
		Medial	18.22±1.46%	60.26±3.27%	2.09±1.04%	3.63±0.72%	0.18±0.00%	0.38±0.48%	0.54±0.39%	3.06±0.47%	10.10±3.31%	1.55±1.53%
		Distal	28.40±1.70%	56.20±1.78%	0.76±0.80%	2.28±0.63%	0.07±0.14%	4.49±1.26%	1.25±0.44%	2.23±0.63%	4.27±0.52%	0.07±0.14%
	2mm Particles	Proximal	6.48±1.62%	26.18±2.35%	2.58±1.22%	7.16±0.80%	0.00±0.00%	0.05±0.12%	1.00±0.58%	6.10±1.60%	49.71±3.70%	0.73±0.53%
		Medial	15.85±2.67%	47.89±2.66%	1.70±0.68%	6.00±4.39%	0.00±0.00%	0.00±0.00%	1.61±0.91%	4.78±1.90%	21.71±3.59%	0.45±0.46%
		Distal	28.66±1.55%	50.94±3.56%	2.96±0.54%	1.32±0.93%	0.00±0.00%	0.23±0.16%	0.28±0.22%	2.95±0.78%	12.60±2.48%	0.06±0.14%
4mmBT Shunt	1mm Particles	Proximal	12.26±1.41%	33.72±3.61%	4.49±0.54%	11.94±2.72%	0.09±0.13%	1.19±0.25%	1.95±0.79%	6.70±1.07%	27.32±4.02%	0.34±0.55%
		Medial	23.63±2.16%	56.31±3.59%	1.60±0.90%	4.43±1.38%	0.22±0.48%	1.53±0.87%	0.55±0.69%	2.93±0.69%	8.67±1.96%	0.13±0.30%
		Distal	31.45±1.25%	52.11±2.23%	1.46±0.86%	1.92±0.86%	0.29±0.24%	5.47±1.66%	0.55±0.52%	1.93±0.73%	4.81±1.46%	0.00±0.00%
	2mm Particles	Proximal	9.46±0.51%	26.15±2.78%	1.81±0.52%	6.03±0.68%	0.00±0.00%	0.00±0.00%	0.89±0.30%	5.25±1.04%	50.16±3.86%	0.25±0.45%
		Medial	14.68±2.14%	50.72±1.22%	1.63±1.12%	5.07±1.40%	0.00±0.00%	0.00±0.00%	1.36±0.75%	6.52±2.09%	19.54±1.07%	0.47±0.33%
		Distal	31.92±1.91%	51.75±1.52%	3.41±1.03%	0.91±0.92%	0.00±0.00%	0.00±0.00%	0.44±0.39%	2.30±0.85%	9.21±1.94%	0.06±0.14%

Table 11: Embolization Rates for Various Shunt/Particle Size (Patient Specific, 90% Stenosis) Including Variance

			RSA	RCA	LCA	LSA	LcorA	RcorA	RPA	LPA	DA	inlet
3mmBT Shunt	1mm Particles	Proximal	11.32±1.85%	13.82±1.94%	3.50±0.85%	1.72±0.91%	0.54±0.44%	0.29±0.32%	0.47±0.43%	2.53±0.50%	16.66±1.53%	49.15±3.48%
		Medial	15.35±2.05%	17.56±2.25%	3.21±1.18%	0.77±0.40%	1.02±0.43%	0.46±0.19%	0.21±0.30%	2.79±0.50%	13.09±1.22%	45.54±1.94%
		Distal	17.18±2.68%	14.36±2.53%	9.27±1.67%	1.43±0.47%	6.99±1.58%	2.29±0.68%	0.32±0.52%	4.20±1.62%	13.28±1.69%	30.69±3.90%
	2mm Particles	Proximal	6.93±1.46%	7.28±2.25%	7.63±1.47%	2.21±1.10%	1.06±0.64%	0.46±0.41%	1.95±0.69%	16.71±1.61%	29.73±3.44%	26.05±2.24%
		Medial	9.02±1.47%	12.74±2.68%	8.67±2.08%	2.00±1.18%	2.34±0.85%	1.04±0.48%	2.89±0.53%	10.31±1.16%	15.68±0.95%	35.30±1.06%
		Distal	10.55±2.00%	10.43±2.11%	11.66±1.58%	1.23±0.85%	4.94±0.41%	2.59±0.64%	2.70±1.40%	10.83±2.83%	12.24±2.47%	32.83±4.17%
3.5mmBT Shunt	1mm Particles	Proximal	8.02±1.18%	21.90±1.98%	5.15±0.80%	8.83±1.33%	2.22±0.81%	0.61±0.45%	1.09±0.62%	2.98±1.11%	32.14±1.60%	17.06±3.41%
		Medial	11.07±1.17%	38.15±1.86%	6.35±1.01%	6.63±0.88%	1.57±0.77%	0.36±0.23%	1.31±0.51%	3.77±1.46%	15.37±2.03%	15.41±1.75%
		Distal	18.50±1.50%	21.27±3.44%	13.65±2.54%	6.60±1.28%	8.03±1.45%	1.58±0.45%	1.68±1.37%	2.98±1.48%	16.96±2.49%	8.75±2.31%
	2mm Particles	Proximal	6.18±1.27%	10.21±1.46%	7.33±1.69%	5.63±1.45%	1.83±0.82%	1.35±0.69%	7.68±1.94%	11.64±2.67%	35.28±3.66%	12.87±2.88%
		Medial	6.46±1.05%	15.02±2.63%	13.28±1.52%	4.61±0.30%	4.33±1.10%	2.35±1.14%	2.58±1.02%	7.30±1.03%	21.94±2.42%	22.11±2.05%
		Distal	12.04±1.53%	12.16±1.33%	17.30±1.14%	3.07±0.59%	4.26±1.20%	2.90±1.16%	2.90±1.01%	8.56±2.30%	21.20±3.10%	15.62±1.03%
4mmBT Shunt	1mm Particles	Proximal	6.55±1.08%	22.23±1.83%	4.71±0.99%	11.51±2.57%	2.72±0.76%	0.60±0.45%	1.14±1.27%	3.01±1.15%	29.68±5.66%	17.85±3.31%
		Medial	9.95±1.56%	42.05±3.49%	7.57±2.76%	7.00±1.59%	1.52±0.53%	0.28±0.23%	1.27±0.85%	4.68±0.52%	15.20±3.38%	10.47±2.38%
		Distal	18.93±2.57%	27.03±2.27%	19.44±2.86%	5.59±2.10%	6.01±1.79%	1.24±0.43%	1.29±0.24%	3.25±1.26%	11.12±2.12%	6.10±1.01%
	2mm Particles	Proximal	3.66±0.60%	13.13±1.49%	5.27±1.36%	5.17±1.87%	2.85±1.05%	1.45±0.83%	7.27±2.19%	11.72±3.60%	34.80±6.65%	14.68±2.62%
		Medial	5.76±1.32%	17.58±3.23%	9.22±1.36%	3.53±1.32%	5.22±1.10%	4.33±0.68%	2.45±0.53%	8.48±4.73%	19.56±1.96%	23.87±3.26%
		Distal	11.75±2.48%	15.21±6.01%	20.11±2.02%	2.91±0.73%	5.74±1.75%	3.97±1.00%	1.81±0.74%	8.23±1.42%	18.40±3.83%	11.88±2.85%

Table 12: Embolization Rates for 3.5mm Shunt Size and Various Particle Size (Nominal, 90% Stenosis) Including Variance

			RSA	RCA	LCA	LSA	LcorA	RcorA	RPA	LPA	DA	inlet
3.5mmBT Shunt	1mm Particles	Proximal	16.02±1.07%	10.89±1.28%	2.52±0.57%	4.65±0.87%	1.04±0.63%	1.31±0.45%	25.42±3.16%	13.86±3.85%	23.89±3.05%	0.40±0.41%
		Medial	25.38±3.71%	9.17±1.52%	2.15±0.83%	2.73±1.18%	0.52±0.74%	1.39±1.07%	14.90±1.62%	17.44±4.15%	26.31±3.16%	0.00±0.00%
		Distal	9.48±3.40%	9.09±3.21%	18.39±3.87%	3.56±0.68%	4.51±1.20%	8.68±1.81%	15.29±2.40%	11.33±2.25%	19.67±2.59%	0.00±0.00%
	2mm Particles	Proximal	6.66±2.09%	7.03±1.73%	7.16±1.24%	3.98±1.40%	2.07±0.73%	4.50±1.49%	44.00±1.15%	9.32±0.97%	14.84±2.07%	0.46±0.41%
		Medial	6.50±1.32%	6.33±1.53%	16.22±2.82%	2.68±0.86%	2.16±0.35%	4.64±0.87%	13.06±1.94%	11.94±1.48%	33.16±3.66%	3.30±1.46%
		Distal	5.98±0.84%	12.43±3.02%	16.54±2.25%	3.04±1.34%	4.50±1.46%	7.54±1.40%	13.96±1.47%	7.26±0.54%	27.07±1.27%	1.66±1.14%

Table 13: Embolization Rates for 3.5mmBT Shunt and Various Particle Size and Geometry Option (Patient Specific, No Stenosis) Including Variance

			RSA	RCA	LCA	LSA	LcorA	RcorA	RPA	LPA	DA	inlet
OPT 1	1mm Particles	Proximal	6.33±1.80%	21.24±2.45%	16.50±2.92%	22.27±2.63%	0.06±0.15%	0.73±0.76%	4.49±0.66%	3.39±0.68%	24.78±1.79%	0.19±0.30%
		Medial	12.80±1.54%	46.90±2.33%	7.62±1.80%	14.25±2.08%	0.15±0.21%	1.17±0.87%	1.56±0.68%	2.55±0.95%	12.93±1.25%	0.07±0.16%
		Distal	22.69±1.70%	59.57±1.98%	2.17±0.82%	5.58±1.42%	0.48±0.53%	1.25±0.64%	0.46±0.04%	2.53±0.56%	5.28±1.17%	0.00±0.00%
	2mm Particles	Proximal	12.27±1.68%	14.69±1.56%	10.48±1.23%	7.40±1.83%	0.40±0.23%	2.35±1.11%	15.53±1.68%	9.32±2.00%	20.08±2.05%	7.46±2.35%
		Medial	24.29±1.41%	35.75±2.10%	17.87±1.22%	2.11±0.73%	0.43±0.36%	3.04±1.51%	2.30±0.98%	2.21±0.91%	7.70±1.69%	4.29±1.74%
		Distal	23.24±1.31%	47.10±2.71%	8.99±1.28%	1.43±0.85%	0.54±0.43%	2.94±0.78%	2.82±1.27%	4.12±1.27%	7.74±1.45%	1.08±0.73%
OPT 2	1mm Particles	Proximal	8.26±1.59%	11.11±1.34%	6.56±1.55%	8.44±1.59%	0.06±0.13%	0.84±0.63%	4.11±0.55%	7.09±1.87%	31.95±2.60%	21.59±2.06%
		Medial	18.65±2.60%	38.14±3.27%	8.29±1.47%	6.74±1.45%	0.15±0.21%	1.02±0.76%	2.00±0.80%	5.75±1.05%	15.21±2.71%	4.07±1.26%
		Distal	26.28±2.95%	55.78±2.64%	4.76±0.95%	1.59±0.72%	0.24±0.27%	2.81±1.08%	1.12±0.57%	2.70±0.77%	4.65±1.09%	0.06±0.13%
	2mm Particles	Proximal	13.06±1.62%	6.96±1.23%	6.44±1.30%	2.59±0.79%	0.33±0.19%	1.00±0.45%	4.31±0.89%	5.08±0.57%	20.32±2.42%	39.91±1.68%
		Medial	27.44±1.76%	20.72±2.15%	10.13±1.86%	2.77±0.45%	0.30±0.32%	1.12±0.42%	2.32±0.99%	4.03±1.12%	12.36±1.64%	18.79±2.23%
		Distal	38.91±3.18%	28.29±2.49%	9.34±0.77%	2.06±0.59%	1.00±0.60%	2.90±0.47%	1.50±0.53%	1.47±0.97%	9.34±1.46%	5.18±1.32%
OPT 3	1mm Particles	Proximal	8.05±2.41%	7.21±2.12%	5.38±1.53%	10.41±1.98%	0.60±0.70%	1.68±0.75%	18.87±3.25%	15.36±1.88%	31.84±4.15%	0.60±0.37%
		Medial	11.89±1.21%	10.94±1.39%	5.02±1.36%	8.20±1.16%	0.49±0.51%	2.61±1.01%	16.45±1.67%	17.10±1.89%	26.29±2.27%	1.02±0.34%
		Distal	13.57±1.79%	14.09±1.42%	3.51±0.88%	10.23±0.95%	0.95±0.78%	5.41±1.59%	12.52±2.49%	14.98±2.18%	23.72±2.26%	1.03±0.50%
	2mm Particles	Proximal	6.06±1.04%	9.84±1.53%	12.12±3.30%	2.96±1.01%	0.77±0.48%	5.55±1.84%	20.75±3.21%	15.42±3.20%	22.90±2.92%	3.62±0.86%
		Medial	7.97±1.56%	12.08±1.15%	6.07±1.46%	2.03±0.97%	1.11±0.45%	7.10±0.78%	24.05±1.86%	21.64±1.57%	16.05±1.39%	1.91±0.39%
		Distal	10.65±0.74%	11.04±1.16%	6.81±0.80%	4.28±1.23%	1.47±0.61%	11.72±1.23%	16.62±2.53%	12.11±1.27%	22.18±2.59%	3.13±0.79%

Table 14: Chi-Square Calculation Table Example (Patient Specific, No Stenosis)

Chi Square Calculation

			RSA	RCA	LCA	LSA	LcorA	RcorA	RPA	LPA	DA	inlet	
3mmBT Shunt	1mm Particles	Proximal	0.0004	0.0761	0.3079	1.2201	0.0009	0.0028	0.0032	0.0111	0.0687	0.0134	1.7045
		Medial	0.0002	0.7898	0.0601	0.1314	0.0003	0.0042	0.0082	0.0007	0.0129	0.0002	1.0079
		Distal	0.2478	0.6445	0.0020	0.0031	0.0010	0.0003	0.2372	0.0003	0.0383	0.0033	1.1779
	2mm Particles	Proximal	0.0001	0.0037	0.0504	0.0845	0.0003	0.0006	0.0032	0.0257	1.1891	0.1147	1.4724
		Medial	0.0159	0.1733	0.0511	0.0179	0.0003	0.0050	0.0006	0.0135	0.3592	0.0159	0.6527
		Distal	0.3271	0.2759	0.0118	0.0027	0.0003	0.0018	0.0001	0.0026	0.0377	0.0002	0.6602
3.5mmBT Shunt	1mm Particles	Proximal	0.0022	0.0357	0.0085	0.1363	0.0003	0.0061	0.0224	0.1863	0.4589	0.1911	1.0479
		Medial	0.0974	0.6111	0.0026	0.0011	0.0082	0.0003	0.0000	0.0058	0.0000	0.0444	0.7710
		Distal	0.4266	0.4856	0.0034	0.0019	0.0005	0.3160	0.0087	0.0003	0.0354	0.0021	1.2806
	2mm Particles	Proximal	0.0066	0.0048	0.0084	0.0557	0.0003	0.0040	0.0035	0.0855	1.5069	0.0047	1.6804
		Medial	0.0541	0.2737	0.0004	0.0287	0.0003	0.0050	0.0202	0.0394	0.1264	0.0004	0.5485
		Distal	0.4382	0.3445	0.0151	0.0097	0.0003	0.0015	0.0014	0.0047	0.0051	0.0022	0.8226
4mmBT Shunt	1mm Particles	Proximal	0.0126	0.0514	0.0620	0.2602	0.0014	0.0093	0.0352	0.1120	0.2811	0.0000	0.8253
		Medial	0.2434	0.4887	0.0001	0.0063	0.0126	0.0211	0.0000	0.0045	0.0026	0.0012	0.7806
		Distal	0.5709	0.3737	0.0000	0.0041	0.0256	0.4905	0.0000	0.0000	0.0292	0.0033	1.4974
	2mm Particles	Proximal	0.0003	0.0047	0.0008	0.0293	0.0003	0.0050	0.0020	0.0537	1.5420	0.0002	1.6383
		Medial	0.0375	0.3391	0.0002	0.0135	0.0003	0.0050	0.0117	0.1037	0.0828	0.0005	0.5943
		Distal	0.5947	0.3647	0.0256	0.0150	0.0003	0.0050	0.0003	0.0005	0.0012	0.0022	1.0094
			3.0762	5.3410	0.6104	2.0216	0.0532	0.8837	0.3579	0.6503	5.7774	0.4001	38.3436

Alpha	0.005
DOF	4
to Exceed	14.86

REFERENCES

Akintuerk, H, et al. "Stenting Of The Arterial Duct And Banding Of The Pulmonary Arteries - Basis For Combined Norwood Stage I And II Repair In Hypoplastic Left Heart." *Circulation* 105.9 (n.d.): 1099-1103. Science Citation Index. Web. 26 Jan. 2017.

Ceballos, Andres. "A Coupled CFD-Lumped Parameter Model Of The Human Circulation. [Electronic Resource]: Elucidating The Hemodynamics Of The Hybrid Norwood Palliative Treatment And Effects Of The Reverse Blalock-Taussig Shunt Placement And Diameter." n.p.: Orlando, FL. University of Central Florida, 2015. *UCF Libraries Catalog.* Web. 28 Jan. 2017.

Chan, MG, et al. "Evaluation Of Expanded Polytetrafluoroethylene-Covered Stents For The Treatment Of Venous Outflow Stenosis In Hemodialysis Access Grafts." *Journal Of Vascular & Interventional Radiology* 22.5 (2011): 647-653. CINAHL Plus with Full Text. Web. 26 Jan. 2017.

Chesnutt, JKW, and HC Han. "Platelet Size And Density Affect Shear-Induced Thrombus Formation In Tortuous Arterioles." *Physical Biology* 10.5 (n.d.): Science Citation Index. Web. 26 Jan. 2017.

Honjo, Osami, and Christopher A Caldarone. "Hybrid Palliation For Neonates With Hypoplastic Left Heart Syndrome: Current Strategies And Outcomes." *Korean Circulation Journal* 40.3 (2010): 103-111. MEDLINE. Web. 26 Jan. 2017.

“Hypoplastic Left Heart Syndrome.” Nationwide Children's, *Nationwide Children's Hospital*,0020. Accessed 28 January 2017.

“Index of /~mga/401/tables” *Penn State,* 5 Nov. 2006, http://sites.stat.psu.edu/~mga/401/tables/Chi-square-table.pdf

Jones, James. “Statistics: Lecture Notes.” *Richland Community College*, https://people.richland.edu/james/lecture/m170/ch12-int.html. Accessed 28 January 2017.

May, Frauke, et al. "Fxiia Inhibitor Rha-Infestin-4: Safe Thromboprotection In Experimental Venous, Arterial And Foreign Surface-Induced Thrombosis." *British Journal Of Haematology* 5 (2016): 769. Academic OneFile. Web. 25 Jan. 2017.

Maxey, Martin R. and James J. Riley. "Equation of Motion for a Small Rigid Sphere in a Nonuniform Flow." *Physics of Fluids (00319171)*, vol. 26, no. 4, Apr. 1983, p. 883 - 889.

Monagle, Paul. "Thrombosis In Children With BT Shunts, Glenns And Fontans." *Progress In Pediatric Cardiology 21. Hemostasis Issues in Cardiovascular Medicine* (2005): 17-21. ScienceDirect. Web. 26 Jan. 2017.

Osorio, AF, et al. "Computational Fluid Dynamics Analysis Of Surgical Adjustment Of Left Ventricular Assist Device Implantation To Minimise Stroke Risk." *Computer Methods In Biomechanics And Biomedical Engineering* 16.6 (n.d.): 622-638. Science Citation Index. Web. 28 Jan. 2017.

Prather, Ray. “A Multi-Scale CFD Analysis Of Patient-Specific Geometries To Tailor LVAD Cannula Implantation Under Pulsatile Flow Conditions [Electronic Resource]: An

Investigation Aimed At Reducing Stroke Incidence In Lvads" n.p.: Orlando, FL. University of Central Florida, 2015. *UCF Libraries Catalog*. Web. 28 Jan. 2017.

Reddy, J. N. *An Introduction to Continuum Mechanics*. 2nd ed. New York: Cambridge U Press, 2013. Print.

Ruiz, Carlos E., et al. "Brief Report: Stenting Of The Ductus Arteriosus As A Bridge To Cardiac Transplantation In Infants With The Hypoplastic Left-Heart Syndrome." *The New England Journal Of Medicine* 22 (1993): 1605. General Reference Center Gold. Web. 26 Jan. 2017.

Shadden, SC, and S Hendabadi. "Potential Fluid Mechanic Pathways Of Platelet Activation." *Biomechanics And Modeling In Mechanobiology* 12.3 (n.d.): 467-474. Science Citation Index. Web. 26 Jan. 2017.